# Chasing anisotropy in the Austin Chalk and Eagle Ford shale formations: azimuthal processing challenges and considerations

*Peng Cheng, Mike Perz*, Femi Ogunsuyi, Frank Meng, and Xinxiang Li, Arcis Seismic Solutions, A TGS Company; William Keller and Victor Kriechbaum, EnerVest, Ltd.*

**Summary**

A 3D land seismic survey from south central Texas was processed using an azimuth-friendly flow, and subsequent azimuthal velocity inversion (VVAZ) was performed in order to characterize the subsurface anisotropy. The resulting anisotropy maps show a strong correlation with production data and therefore demonstrate successful application of the VVAZ technology. This paper examines those key elements of the data processing and of the VVAZ strategy which led to this successful result, namely multi-domain pre-migration noise attenuation, 5D interpolation to an output grid which is regularly sampled across offset and azimuth coordinates, post-migration noise attenuation operating directly in the coordinate planes created by the above 5D interpolation, careful time-shift estimation and maximum incidence angle selection during the azimuthal RMS parameter estimation process, and finally careful testing of the impact of the number of 5D-interpolated azimuths on the quality of the azimuthal interval property estimates.

**Introduction**

The data set under study is a 50 sq. mile subset of a tightly-sampled, 195 fold, 710 sq. mile 3D seismic survey which was acquired in 2015 over a portion of Giddings Field and the eastern extension of the Eagle Ford shale play. The zone of interest is between the top of the Austin Chalk and the top of the Buda limestone, an approximately 1000 ft interval that spans both the Austin Chalk and Eagle Ford formations. At the outset of the project, it was suspected that vertically pervasive fractures, local anomalies in the in-situ horizontal stress field, or both could place a significant control on hydrocarbon production, and accordingly an effort was undertaken to characterize the interval velocity azimuthal anisotropy using the surface seismic data. Processing was carried out according to an azimuthally-AVO-compliant framework which sought to preserve kinematic and amplitude signal variations across both offset and azimuth coordinates. After processing through anisotropic (VTI) pre-stack time migration (PSTM), the data were submitted to VVAZ inversion via the Generalized Dix Inversion (Grechka et al., 1999), a methodology which estimates azimuthal interval fast and slow velocities and fast-velocity orientation (*Vint_fast*, *Vint_slow*, $\phi$*_int*, respectively) from their corresponding RMS counterparts (*Vrms_fast*, *Vrms_slow*, $\phi$*_rms*, respectively). The resulting interval anisotropy maps were then compared to production maps. Details of this comparison are presented in a companion paper (Keller et al., 2017), but the main point in the context of the present work is that a strong correlation was observed between production and the estimated azimuthal anisotropy properties. In particular, regions exhibiting relatively low values of *Vint_slow* and/or values of strong anisotropy (i.e., as evidenced by the magnitude of *Vint_fast* minus *Vint_slow*) were observed to correspond to regions of high production (mostly gas).

Not only does this happy observation of strong correlation between VVAZ attribute maps and production data imply that VVAZ inversion holds great promise as a tool for optimizing future production in the area, it also serves as implicit validation of the processing and inversion methodologies that were used to produce the maps. It is this latter consideration that constitutes the primary motivation behind the writing of this paper, and in the following work we discuss those elements of the processing flow and of the VVAZ inversion which we believe contributed most significantly to the successful outcome.

**Description of key methodologies**

Pre-migration noise attenuation

Pre-migration noise attenuation was performed in various domains using an AVO-compliant philosophy. Most crticially, this noise attenuation avoided any multi-channel processes which risk smearing signal across the azimuth domain. While it is relatively easy to naturally avoid such smearing at the linear noise and noise-burst suppression stages, particular care is required at the random noise attenuation stage. To this end, our random noise attenuation approach entailed running fxy deconvolution in the cross-spread domain, a domain for which the offset and azimuth coordinates vary slowly across neighboring traces within the processing block. This fxy deconvolution was then combined with an adaptive signal addback scheme to ensure preservation of subtle azimuthal signal signatures.

5D interpolation and output geometry considerations

Implementation details of 5D interpolation can vary widely, but one common practice (and the one adopted here) is to define the 5D internal computational grid in a mixed Cartesian-polar coordinate system: (i.e., *cmp-x, cmp-y, offset, azimuth*) according to the grid sampling recommended by Trad (2009). This choice of computational grid naturally produces a high-quality interpolated set of CMP gathers with regular sampling across both offset and azimuth indices, and with fine sampling of the offset coordinate in particular. In the case of the present work, we simply grouped these interpolated CMP gathers by common offset-azimuth indices in order to produce single fold common-offset-vector (COV) ensembles which were in turn input to PSTM. Note that this process of direct grouping into COV's avoids a circuitous approach, adopted by many practioners, comprising the following steps: (i) interpolation using the above internal computational grid; (ii) casting the interpolated data from (i) onto a "surface-referenced" grid consisting of a set of finely sampled source and receiver lines; and (iii) performing offset-vector-tiling (OVT) on these surface-referenced data to produce single-fold, azimuth-and-offset-localized data subsets which are in turn input to PSTM. Although this "5D+OVT" approach is suitable for creating the surface-consistent data configurations required for certain imaging methods like reverse-time-migration, it is unnecessary for the Kirchhoff algorithm which is commonly used in azimuthal processing workflows, including the present one (Perz and Cary, 2012).

An advantage of the 5D approach employed here (i.e., direct grouping into COV's) is that it produces a regular distribution of polar offsets, which in turn permits the use of some powerful post-migration noise suppression techniques described in the next subsection. The differences in offset and azimuth distributions between the present interpolation scheme and the 5D+OVT approach are illustrated in Figure 1. The snail gather of the 5D+OVT approach shows an irregular offset distribution (Figure 1a) and also a relative dearth of near offsets (blue graph at top). By contrast, data created by direct grouping of the 5D-interpolated data into COV's exhibit a perfectly regular, and finely sampled, offset distribution (see Figure 1b for data display in common-offset-common-azimuth (COCA) mode with primary sort key offset, and Figure 1c for same data displayed in CACO mode with primary sort key azimuth). The regular offset distribution is particularly obvious in the CACO display, where it should be apparent that each of the four data subsets correspond to a single constant azimuth "spoke".

Post-migration spoke-by-spoke noise attenuation

Returning to Figure 1c, it is evident that the residual linear noise is particularly well-organized on each individual azimuth spoke. We can exploit this fact by applying traditional 2D f-k filtering piecewise on each spoke (where, crucially, the fine offset sampling precludes spatial aliasing) to attack the noise. In practice we combine the f-k filtering with an adaptive signal addback scheme to ensure no distortion of primary reflections. Though not shown here, we also observe strong organization of multiple energy on azimuth spokes, paving the way for an analogous spoke-by-spoke demultiple strategy. Figure 2 shows the application of the spoke-by-spoke denoising to the test subvolume. Figure 2a shows the input COCA gather exhibiting contamination by both linear noise and multiple energy and Figure 2b shows the final denoised result. Clearly the denoise strategy has worked very well: the underlying signal has been unveiled and exhibits very strong azimuthal variation as evidenced by the pronounced "sinusoidal wobble" at far offsets; moreover, inspection of the underlying noise models (i.e., which were subtracted from the input data) in Figures 2c and 2d show no hint of residual primary signal. We note with interest, if not surprise, that these latter two noise models exhibit significant azimuthal variation themselves. Finally, we note that a primitive 2D noise attenuation operating across the offset coordinate in an "azimuth-blind" fashion would surely produce very poor results as the azimuthal variation in both signal and noise would be smeared in the process, resulting in poor noise removal and signal distortion.

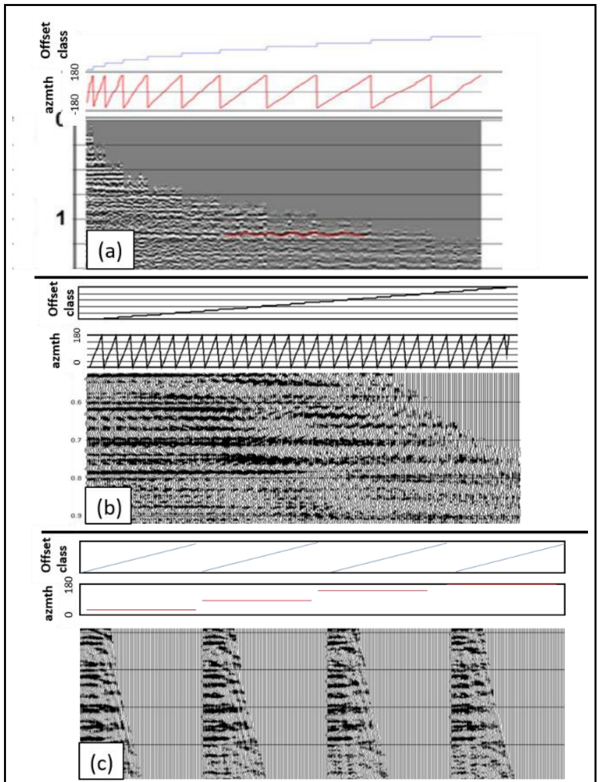


Figure 1: Examples of CMP gathers after 5D interpolation + PSTM: (a) snail gather after 5D+OVT+PSTM (west Texas, excerpted from McCarthy et al., 2016); (b) COCA gather after direct migration of data from a 5D computational grid with 30° azimuth interval and 40 m offset interval (central Alberta, data courtesy of Arcis Seismic Solutions, A TGS Company); (c) same data as (b), except ordered in CACO mode—note only 4 of the 6 azimuths are shown here .

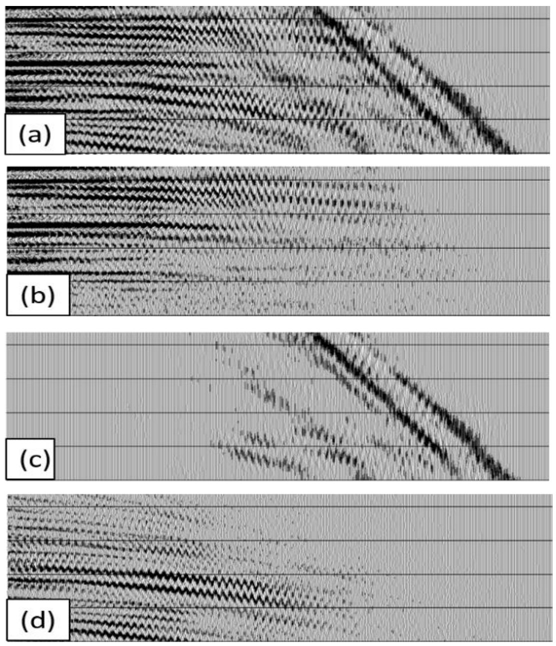


Figure 2: Spoke-by-spoke noise attenuation. (a) input migrated COCA; (b) final denoised COCA after linear noise and de-multiple steps; (c) noise estimated from linear denoise; (d) multiples estimated from de-multiple process. Seismic data is the proprietary property of Seitel, Inc.

VVAZ inversion considerations

*(i) Time shift estimation*

After spoke-by-spoke noise removal, the migrated common-image-point (CIP) gathers were input to an algorithm which estimates the $\Delta t$ time shifts giving rise to the sinusoidal wobble observed in Figure 2b. Estimation of these $\Delta t$'s required careful consideration on the test subvolume because of the large amount of azimuthal anisotropy together with the uncommonly large incident angle range. While the large range is ultimately a fortunate occurrence (because the associated oblique ray angles are quite sensitive to the effects of azimuthal anisotropy), it introduces a large amount of systemic disparity between near and far offset waveforms which can, in turn, pose challenges for $\Delta t$-estimation. Figure 3a shows a migrated CIP exhibiting extreme azimuthal anisotropy for which $\Delta t$ time shifts are estimated via two different approaches. The first approach is the "AVO-projected pilot" technique of Zheng et al., 2008, an approach which honors offset-dependent amplitude effects but not waveform changes. Figure 3b shows the result after first estimating then applying, $\Delta t$'s from the this approach (note that a perfect result would imply perfect gather flattening). While the algorithm has done a good job of flattening up to 45º, severe cycle-skipping is observed at the higher angles (blue ellipse). Figure 3c shows the result of applying $\Delta t$'s estimated via an alternative "sliding window" approach

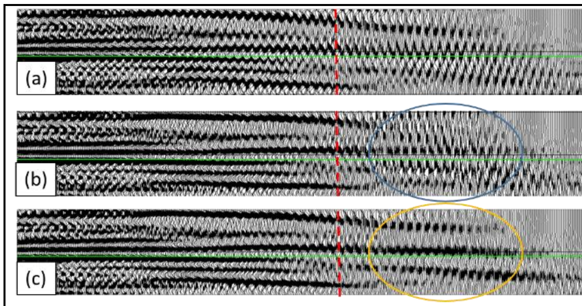


Figure 3: Comparisoin of $\Delta t$ time shift estimation approaches .(a) input data (migrated COCA); (b) after flattening with $\Delta t$'s computed via AVO-projected pilot algorithm c) after flattening with $\Delta t$'s computed via sliding window approach. Red dashed line shows 45° angle. Seismic data is the proprietary property of Seitel, Inc.

which explicitly adapts to offset-dependent waveform changes. Clearly it has done an excellent job of flattening, even at the highest propagation angles (orange ellipse).

*(ii) Maximum angle in RMS parameter estimation*

Once computed, the $\Delta t$'s are input to an elliptical curve-fitting process (Grechka and Tsvankin, 1998) to estimate azimuthal RMS properties *Vrms_fast*, *Vrms_slow*, *$\phi$_rms*. One key input parameter in the curve-fitting process is the maximum incidence angle for which the $\Delta t$'s are inverted and its optimal selection proved surprisingly difficult in the present work. Figure 4a shows a final migrated CIP gather in COCA mode, while Figure 4b shows its counterpart after azimuthal NMO correction in the case that the associated azimuthal RMS inversion only considered $\Delta t$'s corresponding to a maximum incidence angle of 40°. Clearly the wobble associated with mid-range offsets (blue ellipse) is well-collapsed; however, the far offset wobble (red ellipse) has unfortunately been accentuated. Figure 4c shows the azimuthal NMO correction based on a 65° maximum inversion angle; in this case the far offset wobble is nicely reduced while the mid-range wobble has been exacerbated. This tradeoff between optimal mid and near offset flattening proved impossible to perfectly manage, and in the end it was decided that a 60° angle be used in the production run. Possible explanations for the existence of this tradeoff are: (a) the fact that the elliptical moveout approximation loses its validity at high propagation angles, (b) the existence of lateral velocity heterogeneity in the overburden or (c) a combination of both. Perhaps not surprisingly, the downstream-generated azimuthal interval maps show significant variation depending on the choice of this maximum angle parameter (Figure 5).

*(iii) Impact of number of azimuths*

Lynn (2011) demonstrated via synthetic experiments that the quality of the azimuthal RMS parameter estimates can vary with the number of input azimuths (with reliability improving with increasing number), and, correspondingly that the number of azimuths may have a profound impact on the quality of the final azimuthal interval estimates. His experimental approach, while scientifically sound, did not consider the effects of 5D interpolation, a relatively new inclusion in azimuthal processing flows which introduces a complex interplay between signal-to-noise enhancement, interpolated image quality, and azimuth smearing. In order to study the effect of the number of output azimuths from 5D interpolation on the quality of the estimated azimuthal interval properties, we devised a synthetic experiment.

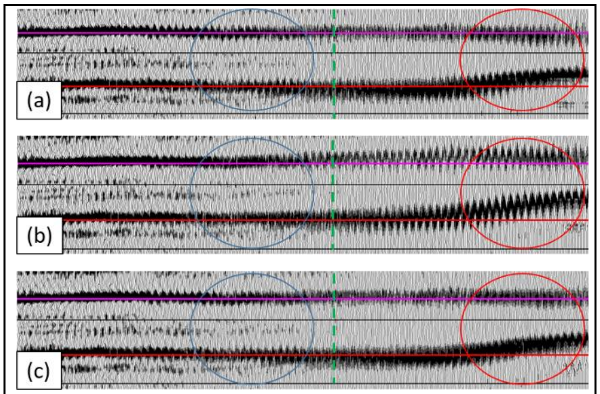


Figure 4: COCA's before and after azimuthal NMO correction with 45° angle shown in dashed green. (a) data before correction; (b) after correction via azimuthal RMS property inversion with maximum angle of 40°; (c) same as (b), except a maximum angle of 65° was used.

Specifically we considered the same azimuthally anisotropic earth model as Lynn (2011) and we performed forward modeling to create synthetic traces (i.e., containing anisotropic traveltime effects) based on the real survey geometry of the test subvolume. We added random noise to this synthetic data set and submitted the noisy data to 5D interpolation for several trial output-azimuth configurations.

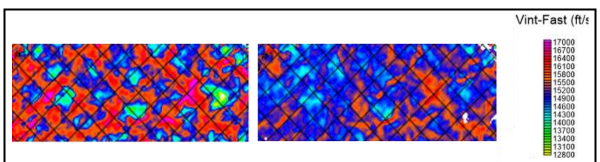

Figure 5: Azimuthal interval maps of *Vint_fast* computed using two different choices for maximum incident angle in the upstream azimuthal RMS parameter estimation.. (left) 40° maximum angle; (right) 60° maximum angle. Images courtesy of Lynn Inc.

Next, for each post-5D output-azimuth configuration we estimated $\Delta t$ shifts, performed the elliptical curve fitting to compute RMS azimuthal parameters, and finally executed the Generalized Dix Inversion to estimate the interval azimuthal parameters. Results are shown in Table 1, where it is clear that quality of the Generalized Dix Inversion result after 5D interpolation does not improve with increasing azimuth. In fact, quality actually *degrades* with increasing azimuth, an observation which is likely due to the fact that 5D interpolation struggles with extreme, and regular, upsampling across any of its coordinates (in this case azimuth). Based on the results of this testing, 6 azimuths were output from 5D interpolation in the production run.

| number of azimuths | % aniso (estimated) | % aniso (true) | $\varphi_{Vfast}$ (deg.) (estimated) | $\varphi_{Vfast}$ (deg.) (true) |
|---|---|---|---|---|
| 6 | 0.02100 | 0.02674 | 102.4 | 100.2 |
| 10 | 0.03003 | 0.02674 | 119.9 | 100.2 |
| 20 | 0.01429 | 0.02674 | 118.4 | 100.2 |

Table 1: Synthetic testing of azimuthal interval property estimation for various trial post-5D output-azimuth configurations. Results are compared against the "true" parameters defined in Lynn (2011). Here "% aniso" is defined as (*Vfast_int* - *Vslow_int*)/*Vfast_int*.

## Conclusions

Careful azimuth-friendly processing and VVAZ inversion were performed on a data set exhibiting a wide range of incident angles, resulting in successful characterization of anisotropy. Key steps in processing were: azimuthally-AVO-compliant pre-migration noise attenuation, 5D interpolation to a set of regularly sampled azimuth spokes, and spoke-by-spoke post-migration noise attenuation. Key considerations in VVAZ inversion were: careful attention in time shift estimation, use of a relatively large incident angle in azimuthal RMS property estimation, and finally choosing to output 6 azimuths after 5D interpolation. Future work is aimed at comparing the present PSTM-based anisotropy characterization to one obtained through orthorhombic PSDM. The possible benefits of using PSDM instead of PSTM in azimuthal velocity characterization have been discussed by numerous authors, including Goodway (2016), Belguermi et al. (2016) and Brown et al. (2017).

## Acknowledgements

We thank Walt and Heloise Lynn for their help and guidance throughout the project. We thank Enervest, Ltd. and Seitel, Inc. for granting permission to publish this work.

**EDITED REFERENCES**

Note: This reference list is a copyedited version of the reference list submitted by the author. Reference lists for the 2017 SEG Technical Program Expanded Abstracts have been copyedited so that references provided with the online metadata for each paper will achieve a high degree of linking to cited sources that appear on the Web.

**REFERENCES**

Belguermi C., A. Zarkhidze, N. Meddour, H.F. Zeidan, C. Chironi, H. Harkas, and A. Widjiastono, 2016, Apparent azimuthal anisotropy resolved by depth imaging: 86th Annual International Meeting, SEG Expanded Abstracts, 328–331, http://dx.doi.org/10.1190/segam2016-13948733.1.

Brown, M., D. Waibel, S. Schapper, and J. Starr, 2017, Marcellus and Utica Shale PSDM Case Study – Improved Structural Imaging and Rock Properties: 23rd Annual RMAG and DGS 3D Seismic Symposium.

Goodway, W., G. Purdue, and M. Perez, 2016, Pre-stack depth imaging to remove the effects of lateral velocity heterogeneity on time imaging that masquerade as azimuthal anisotropy: Midale EOR Case Study: 5th Annual CSEG Symposium.

Grechka, V., and I. Tsvankin, 1998, 3-D description of normal moveout in anisotropic inhomogeneous media: Geophysics, **63**, 1079–1092, http://dx.doi.org/10.1190/1.1444386.

Grechka, V., I. Tsvankin, and J. Cohen, 1999, Generalized Dix equation and analytic treatment of normal moveout velocity for anisotropic media: Geophysical Prospecting, **47**, 117–148, http://dx.doi.org/10.1046/j.1365-2478.1999.00120.x.

Keller, W., R. Mott, A. Jumper, H. Lynn, W. Lynn, and M. Perz, 2017, Correlation of azimuthal velocity anisotropy and seismic inversion attributes to Austin Chalk production, a south central Texas case study: 87th Annual International Meeting, SEG, Expanded Abstracts, submitted.

Lynn, W., 2011, Azimuthal interval velocity uncertainty: 81st Annual International Meeting, SEG, Expanded Abstracts, 279–283, http://dx.doi.org/10.1190/1.3627776.

McCarthy, A., A.B. Ahmadi, and J. Schneider, 2016, Advanced seismic processing: a case study on imaging in the Delaware Basin: CSEG Geoconvention.

Perz, M., and P. Cary, 2012, 5D interpolation and COV migration: A perfect marriage: CSEG Geoconvention.

Trad, D., 2009. Five-dimensional interpolation: Recovering from acquisition constraints: Geophysics, **74**, no. 6, V123–V132, http://dx.doi.org/10.1190/1.3245216.

Zheng Y., J. Wang, and M. Perz, 2008, Pitfalls and tips for seismic fracture analysis: 78th Annual International Meeting, SEG, Expanded Abstracts, 1531–1535, http://dx.doi.org/10.1190/1.3059205.